Original Paper

Role of Piezo2 in Schwann Cell Volume Regulation and Its Impact on Neurotrophic Release Regulation

Chawapun Suttinont[a]   Katsuyuki Maeno[a]   Mamiko Yano[a]   Kaori Sato-Numata[b]
Tomohiro Numata[b]   Moe Tsutsumi[a]

[a]MIRAI Technology Institute, Shiseido Co., Ltd., Yokohama, Japan, [b]Department of Integrative Physiology, Graduate School of Medicine, Akita University, Akita, Japan

Key Words
Schwann cell • Piezo2 • Mechanoreceptor • Volume regulation • Neurotrophic release

Abstract

Background/Aims: Tactile perception relies on mechanoreceptors and nerve fibers, including c-fibers, Aβ-fibers and Aδ-fibers. Schwann cells (SCs) play a crucial role in supporting nerve fibers, with non-myelinating SCs enwrapping c-fibers and myelinating SCs ensheathing Aβ and Aδ fibers. Recent research has unveiled new functions for cutaneous sensory SCs, highlighting the involvement of nociceptive SCs in pain perception and Meissner corpuscle SCs in tactile sensation. Furthermore, Piezo2, previously associated with Merkel cell tactile sensitivity, has been identified in SCs. The goal of this study was to investigate the channels implicated in SC mechanosensitivity and the release process of neurotrophic factor secretion. *Methods:* Immortalized IFRS1 SCs and human primary SCs generated two distinct subtypes of SCs: undifferentiated and differentiated SCs. Quantitative PCR was employed to evaluate the expression of differentiation markers and mechanosensitive channels, including TRP channels (TRPV4, TRPM7 and TRPA1) and Piezo channels (Piezo1 and Piezo2). To validate the functionality of specific mechanosensitive channels, Ca^{2+} imaging and electronic cell sizing experiments were conducted under hypotonic conditions, and inhibitors and siRNAs were used. Protein expression was assessed by Western blotting and immunostaining. Additionally, secretome analysis was performed to evaluate the release of neurotrophic factors in response to hypotonic stimulation, with BDNF, a representative trophic factor, quantified using ELISA. *Results:* Induction of differentiation increased Piezo2 mRNA expression levels both in IFRS1 and in human primary SCs. Both cell types were responsive to hypotonic solutions, with differentiated SCs displaying a more pronounced response. Gd^{3+} and FM1-43 effectively inhibited hypotonicity-induced Ca^{2+} transients in differentiated SCs, implicating Piezo2 channels. Conversely, inhibitors of Piezo1 and TRPM7 (Dooku1 and NS8593, respectively) had no discernible impact. Moreover, Piezo2 in differentiated SCs appeared to participate in regulatory volume decreases (RVD) after cell swelling induced by hypotonic stimulation. A Piezo2

Tomohiro Numata, Ph.D.
and Moe Tsutsumi, Ph.D.

Department of Integrative Physiology, Graduate School of Medicine, Akita University
1-1-1, Hondo, Akita, 010-8543, Japan,
Tel. +81-(0)18-833-6272,
E-Mail numata@med.akita-u.ac.jp
Shiseido Co., Ltd., MIRAI Technology Institute, 1-2-11, Takashima, Nishi-ku, Yokohama,
220-0011, Japan,
Tel. +81-(0)70-3859-1977, Fax +81-(0)45-590-6019,
E-Mail moe.tsutsumi@shiseido.com

Cellular Physiology and Biochemistry

Cell Physiol Biochem 2024;58:292-310

DOI: 10.33594/000000713
Published online: 8 July 2024

© 2024 The Author(s). Published by
Cell Physiol Biochem Press GmbH&Co. KG

293

Suttinont et al.: Neurotrophic Release Control by Piezo2

deficiency correlated with reduced RVD and prolonged cell swelling, leading to heightened release of the neurotrophic factor BDNF by upregulating the function of endogenously expressed Ca^{2+}-permeable TRPV4. **Conclusion:** Our study unveils the mechanosensitivity of SCs and implicates Piezo2 channels in the release of neurotrophic factors from SCs. These results suggest that Piezo2 may contribute to RVD, thereby maintaining cellular homeostasis, and may also serve as a negative regulator of neurotrophic factor release. These findings underscore the need for further investigation into the role of Piezo2 in SC function and neurotrophic regulation.

Introduction

Schwann cells (SCs), integral glial cells in the peripheral nervous system (PNS), play pivotal roles in supporting axonal growth in peripheral neurons and contribute significantly to axonal regeneration following nerve injuries. SCs exist in two distinct forms: myelinating SCs, which form a unitary association with large axons, and non-myelinating SCs, which enclose multiple small-diameter axons within a single SC, forming Remak bundles, and both types of SCs facilitate action potential conduction [1, 2].

Recent studies have expanded our understanding of SCs, revealing that they have additional functions beyond their traditional roles. SCs have emerged as essential players in mechanical nociception and tactile perception. Specialized nociceptive SCs form a mesh-like network at the subepidermal border and exhibit a tight association with nociceptive nerves. These specialized SCs demonstrate a remarkable mechanosensitivity, transducing mechanical stimuli into pain-like responses in mice [3]. Furthermore, SCs envelop mechanoreceptors such as Meissner's corpuscles that are critical for detecting vibrotactile stimuli in mice [4]. Intriguingly, these mechanosensory functions depend on the myelinating or non-myelinating phenotype of SCs.

Several mechanotransduction channels have been reported in SCs. Piezo1 and Piezo2, for instance, have been implicated in myelin formation, as demonstrated in rat primary cultured SCs and in knockout mouse models [5]. Transient receptor potential (TRP) V4 in non-myelinating SCs has been associated with demyelination following nerve injuries in mice, with functional TRPV4 expression confirmed in cultured mouse SCs [6]. TRPM7 in mouse SCs has been shown to play a role in peripheral neurodegenerative processes in ex vivo sciatic nerve cultures [7, 8]. Additionally, functional TRPA1 expression has been identified in mouse primary SCs, and its involvement in allodynia has been demonstrated, including in cultured rat and human SCs [9, 10].

It is well-established that isolated, cultured SCs display a proliferative phenotype when cultured in media containing defined mitogenic factors. Those SCs exhibit an immature phenotype, especially in the absence of neurons [11]. However, the co-culture of SCs with dorsal root ganglia (DRG) neurons, supplemented with serum and ascorbic acid, prompts their differentiation into a myelinating SC-like phenotype [12]. Furthermore, increasing levels of intracellular cyclic adenosine monophosphate (cAMP) induce the differentiation of SCs in the absence of neurons [13, 14]. However, the mechanisms by which differentiated SCs detect and process mechanical information remain largely unknown. Additionally, there is ample room for further research on the release of neurotrophic factors into the periphery following mechanical stimulation.

In this study, we utilized differentiated IFRS1 SCs and human primary culture SCs to investigate the identification of mechanoreceptors and the release of neurotrophic factors induced by their activation.

Materials and Methods

Cell cultures of IFRS1 SCs and human primary SCs

IFRS1 SCs (immortalized adult Fischer rat SCs) were obtained from Cosmo Bio Co., Ltd., Tokyo, Japan. Human primary SCs (HSCs) were generously provided by Dr. Paula Monje (University of Kentucky) [15, 16]. Human Embryonic Kidney (HEK) 293T cells were kindly provided by Dr. Yasunobu Okada (National Institute for Physiological Sciences).

Primary HSC experiments utilized isolated postmortem adult tissues obtained from a Cell Bank maintained by Kentucky University and those cells were used up to 8 passages. HSC experiments followed strict ethical and safety protocols. The study protocol was further reviewed and approved by the Shiseido MIRAI Institute Ethics Committee according to the National Institutes of Health guidelines and the Helsinki Declaration of Principles (C10424). These HSC cultures were derived from non-pathological neural tissues of individuals aged 10 to 66 years and were thoroughly screened to be free of blood-borne viruses. After HSCs underwent a growth phase in culture, they were purified using magnetically activated cell sorting (MACS) to ensure purity and quality. For the detailed methodology used to produce and bank HSC lines, please refer to previous publications [15, 16].

Cells were maintained at 37°C with 5% CO_2 for HEK293 and IFRS1 SCs and with 8% CO_2 for HSCs, with passages up to 8 used during culture maintenance. All procedures were conducted in a controlled, sterile environment to promote the proliferation and maintenance of IFRS1 SCs, HEK293T cells and HSCs in their respective culture conditions. For cell volume experiments, cells were detached with trypsin, resuspended, and stored in a gently agitated isotonic solution (300 mOsm) for 60 min in a 37°C incubator before use, ensuring consistency in the experimental conditions.

Culture media used included Low-glucose Dulbecco's Modified Eagle's Medium (DMEM) (Thermo Fisher Scientific, MA, USA), High-glucose DMEM (Thermo Fisher Scientific), 0.05% Trypsin-ethylenediamine tetraacetic acid (EDTA) (Thermo Fisher Scientific), 100 × GlutaMAX Supplement (Thermo Fisher Scientific), 10, 000 U/L penicillin-streptomycin (Thermo Fisher Scientific), fetal bovine serum (FBS; Hyclone Laboratories, UT, USA), 1 mol/L-2-[4-(2-hydroxyethyl)piperazin-1-yl]ethanesulfonic acid (HEPES) buffer (Nacalai Tesque, Kyoto, Japan). For the expansion of undifferentiated SCs, the following supplements were utilized: Recombinant human Heregulin β-1 (Thermo Fisher Scientific), Forskolin (Sigma-Aldrich, GmbH, Schnelldorf, Germany). For the differentiation of SCs, the following supplements were employed: cell-permeable cAMP derivative 8-(4-chlorophenylthio) adenosine-3',5'-cyclic monophosphate (CPT-cAMP; Abcam, Cambridge, UK) and ascorbic acid (Nacalai Tesque). To prepare cell culture vessels, Poly-D-Lysine (PDL; Thermo Fisher Scientific) and Laminin solution obtained from mouse Engelbreth-Holm-Swarm (EHS) tumor (FUJIFILM Wako Pure Chemical Corporation, Osaka, Japan) were utilized as coatings.

RNA Isolation and Quantitative reverse transcription polymerase chain reaction (RT-qPCR)

RNAs were isolated using a RNeasy Mini kit (Qiagen, Hilden, Germany) following the manufacturer's instructions. A total of 50 ng RNA was utilized in TaqMan™ Gene Expression Master Mix (Thermo Fisher Scientific) with the following cycling conditions: initial heating at 48°C for 15 min, 95°C for 10 min, followed by 40 cycles of denaturation at 95°C for 15 s and annealing and extension at 60°C for 1 min.

Specific primers were employed to measure relative gene expression levels, targeting p75 neurotrophin receptor (p75NTR), Early Growth Response 2 (KROX20/EGR2), Myelin Basic Protein (MBP), Piezo1, Piezo2, TRPM7, TRPV4 and TRPA1. The mRNA levels were normalized to the housekeeping gene, glyceraldehyde-3-phosphate dehydrogenase (GAPDH). Data analysis was performed using Roche LightCycler 96 software (Roche Diagnostics, Basel, Switzerland) and the comparative cycle threshold (Ct) method ($2^{-\Delta CT}$) for Figs. 1b and 3b, and the ($2^{-\Delta\Delta CT}$) method for Figs. 1c and 3c. RT-qPCR primer sequences were sourced from Thermo Fisher Scientific. qRT-PCR primers used were as follows: rat p75Ntr sequence No. Rn00561634_m1 Ngfr, Krox20 sequence No. Rn00586224_m1 Egr2, Mbp sequence No. Rn01399619_m1 Mbp, Piezo1 sequence No. Rn01432593_m1 Piezo1, Piezo2 sequence No. Rn01491821_m1 Piezo2, Trpm7 sequence No. Rn00586779_m1Trpm7, Trpv4 sequence No. Rn00576745_m1 Trpv4, and Trpa1 sequence No. Rn01473803_m1 Trpa1, b-actin sequence No. Rn00667869_m1 Actb, human Ngfr, nerve growth factor receptor (p75NTR) sequence No. Hs00609976_m1 NGFR, KROX20 sequence No. Hs00166165_m1 EGR2 , MBP sequence No. Hs00921945_m1 MBP, PIEZO1 sequence No. Hs00207230_m1 PIEZO1, PIEZO2 sequence No. Hs00926218_m1 PIEZO2, TRPM7 sequence No. Hs00559080_m1 TRPM7, TRPV4 sequence No. Hs01099348_m1 TRPV4, and TRPA1 sequence No. Hs00175798_m1 TRPA1 and GAPDH sequence No. Hs02786624_g1 GAPDH.

Cellular Physiology and Biochemistry

Cell Physiol Biochem 2024;58:292-310

DOI: 10.33594/000000713
Published online: 8 July 2024

© 2024 The Author(s). Published by
Cell Physiol Biochem Press GmbH&Co. KG

295

Suttinont et al.: Neurotrophic Release Control by Piezo2

Mean cell volume measurements

Mean cell volumes were measured at room temperature by electronic sizing using a Coulter-type cell size analyzer (CDA-500; Sysmex, Hyogo, Japan). Isotonic or hypotonic solutions (300 or 215 mOsmol/kgH$_2$O adjusted by D-mannitol) contained the following components (in mM): 100 NaCl, 5 KCl, 0.4 MgCl$_2$, 0.42 CaCl$_2$, 10 D-glucose and 5 HEPES, with pH adjusted to 7.4 by NaOH. Osmolality was measured accurately using an osmometer (Vapro 5600 Vapor Pressure Osmometer, Wescor EliTech, UT, USA). Relative cell volume was calculated using the equation: relative cell volume = V_A/V_{Ctl}, where V_{Ctl} and V_A represent the mean cell volumes before and after the hypotonic challenge.

Immunocytochemistry

Differentiated and undifferentiated IFRS1 SCs, initially seeded on poly-D-lysine-coated coverslips, underwent a standardized series of treatments. Firstly, they were subjected to two rounds of phosphate-buffered saline (PBS) treatment, then were fixed in 2% paraformaldehyde solution in PBS for 10 min. Afterward, the cells underwent three PBS washes and were subsequently treated with a 0.1% Triton X-100 solution in PBS supplemented with 3% donkey serum for 10 min to facilitate cell membrane permeabilization. Following permeabilization, the cells were subjected to a blocking step involving 3% donkey serum (blocking solution) for 1 h. Subsequently, primary antibodies to MBP (1:500 dilution: sc-271524; Santa Cruz Biotechnology, TX, USA) or to PIEZO2 (1:500 dilution: 8613; ProSci Inc, CA, USA) were applied in the blocking solution for a 2 h incubation period at room temperature. Post-incubation, the cells underwent three PBS washes before being treated with a secondary antibody (Alexa Fluor 488 donkey anti-mouse IgG (H+L), A21202, 1:500 dilution, Thermo Fisher Scientific) or (Alexa Fluor donkey anti-mouse IgG (H+L) or rabbit IgG (H+L); 1:500 dilution Thermo Fisher Scientific). Additionally, 0.02 µM Hoechst 33342 was added and protected from light for 1 h at room temperature. Following the staining step, cells underwent three PBS washes and were subsequently mounted on glass slides using ProLong™ Gold Antifade Mountant (P36930, Thermo Fisher Scientific). The mounted slides with attached cells were observed using an LSM800 confocal laser scanning microscope (Carl Zeiss, Jena, Germany).

Western blotting

IFRS1 SCs and HEK293T cells were cultivated in 6 cm dishes. To obtain the hPiezo2 protein as a positive control for Fig. 6b, a hPIEZO2 expression vector (Vector Builder Inc., IL, USA) was transfected into HEK293T cells and cultured for a period ranging from 36 to 60 h. Cells were then solubilized in radioimmunoprecipitation assay buffer maintained on ice, comprised of 0.1% SDS (Sodium Dodecyl Sulfate), 0.5% sodium deoxycholate, 1% Nonidet P40, 150 mM NaCl, 50 mM Tris-HCl, 1 mM PMSF (phenylmethylsulfonyl fluoride), and Halt Protease Inhibitor Cocktail (Thermo Fisher Scientific) at pH 8.0. The resulting cell lysate was centrifuged at 17, 400 g for 30 min at 4°C. The supernatant obtained was electrophoresed using SDS-PAGE and electrotransferred onto a nitrocellulose membrane (GE Healthcare Life Sciences, IL, USA).

Quantification of protein expression levels was conducted by incubating the membrane with antibodies to PIEZO2 (1:1000 dilution: MA1-10837, Sigma-Aldrich) or α-tubulin (1:2000 dilution: T6074; Sigma-Aldrich), followed by a secondary antibody of mouse IgG (1:3000 dilution, Amersham, Little Chalfont, UK). Chemiluminescence was detected using Amersham's ECL system, followed by incubation with HRP-conjugated sheep Ab (1:3000 dilution: NA931; Merck, Darmstadt, Germany). Immunoreactivity was visualized using ImmunoStar Zeta chemiluminescent reagents (Fujifilm Wako). The chemiluminescence emitted from the membrane was captured using a LumiVision Pro 400EX system (Aisin Seiki Co., Ltd., Aichi, Japan). Quantitative analysis of Western blot results was performed using the ImageJ program [17].

Intracellular Ca^{2+} imaging

SCs were cultured by seeding onto poly-D-lysine (PDL)-coated coverslips with a diameter of 13 mm (Matsunami Glass, Tokyo, Japan). Initially, the cells were cultured in an undifferentiated medium, which was then transitioned to a differentiation medium on the following day. After 2 days of culture, intracellular Ca^{2+} dynamics in individual SCs were examined by ratio imaging using Fura-2-AM (Thermo Fisher Scientific). Prior to taking measurements, the cells were treated for 60 min in an isotonic solution containing a defined concentration of Fura-2-AM. Afterwards, the cells were mounted on coverslips in the experimental chamber. Only cells that showed stable ΔRatio values when measured in an isotonic solution before the procedure were chosen for Ca^{2+} imaging measurements.

Cell responses were captured using CellSens fluorescence ratio imaging software (version 1.18, Evident, Tokyo, Japan). The light emitted from an LED-type light source (pE-340 fura, Cool LED, Andover, UK) was recorded using an inverted microscope (IX81, Evident) equipped with a switching function for a 340/380 nm bandpass filter, thereby allowing ratiometric imaging. All experiments were conducted at room temperature.

The experimental solution contained the following components (in mM): 90 NaCl, 4.5 KCl, 2 $CaCl_2$, 0.3 $MgCl_2$, 10 glucose and 10 HEPES (pH = 7.4). Isotonic (Iso) or hypotonic (Hypo) solutions were adjusted to 300 or 200 mOsmol/kgH_2O using D-mannitol. Osmolality was measured accurately using an osmometer.

Measurements were conducted by establishing a baseline using an isotonic solution (Iso) for 2 min as a control, followed by exposure to a hypotonic solution (Hypo) for 4 min under continuous perfusion. Before hypotonic stimulation, mechanosensitive channel inhibitors, including 30 mM $GdCl_3$ (Tocris Bioscience, Bristol, UK), 20 mM FM™1-43 (Thermo Fisher Scientific), 20 mM Dooku1 (Tocris Bioscience), or 30 mM NS8593 (Merck), 1 mM HC-067047 (Selleck, Houston, US) were pretreated 30 s before the stimulation. All other drugs and chemicals were purchased from Sigma-Aldrich.

Small interfering RNA transfection

HSCs were transfected with 25 nM siRNA targeting human PIEZO2 or non-target siRNA (D-001810-10-05, Horizon Discovery, Cambridge, UK) using Lipofectamine™ LTX Reagent (Thermo Fisher Scientific), following the manufacturer's instructions. In brief, siRNAs and Transfection Reagent were each diluted to 5 µM with Opti-MEM (Thermo Fisher Scientific), mixed and then incubated at room temperature for 20 min. Cells in 24-well plates were fed 500 ml fresh culture medium and overlaid with the transfection mixture. After 24-48 h of transfection, samples were confirmed by qPCR detecting PIEZO2 expression.

Secretome analysis of HSCs

Cell preparation. HSCs were seeded at 4 x 10^5 cells in poly-D-lysine (PDL)/Laminin-coated 6 cm cell culture dishes in undifferentiated medium (FBS decreased to 5%) and changed to differentiated medium the next day. After 2 days of culture, the medium was substituted with differentiated medium without FBS for 4 h before stimulation. Cell samples were gently washed with isotonic solution 3 times to remove FBS before stimulation, as described previously [18]. Subsequently, cells were exposed to either a hypotonic or isotonic solution, and the supernatant was collected for secretome analysis after 10 min of stimulation.

Sample preparation for liquid chromatography-tandem mass spectrometry (LC-MS/MS). An EasyPep™ 96 MS Sample Prep Kit (Thermo Fisher Scientific) was employed for sample preparation utilizing the reagents provided in the kit. The procedure for preparing peptides for MS analysis is as follows: 1.2 mL cooled acetone (six times the volume) was added to 200 µL of the protein sample and incubated at -30°C for 2 h to precipitate proteins. The sample was centrifuged at 16, 000 × g at 4 °C for 10 min, after which the supernatant was removed. Fifty µL cooled 90% acetone was added to the sample and mixed. The sample was centrifuged at 16, 000 × g at 4 °C for 5 min, and the supernatant was removed. The pellet was allowed to dry for 3 min, after which 100 µL Lysis Solution was mixed with the sample to solubilize the pellet. Fifty µL Reduction Solution was added to the sample and mixed. Fifty µL Alkylation Solution was added to the sample and mixed. The sample was then incubated at 95 °C for 10 min to reduce and alkylate the proteins. After incubation, the sample was allowed to cool to room temperature. 50 µL of the reconstituted enzyme solution (0.1 µg/µL of Trypsin/Lys-C Protease Mix) was added to the sample and incubated at 37 °C for 2 h to digest the proteins. After digestion, 50 µL Digestion Stop Solution was mixed to acidify the peptide sample. The sample was purified with the Peptide Clean-up Plate and the supplied solutions to remove contaminants and enzymes. The eluted peptide sample was dried using a vacuum centrifuge, then resuspended in 100 µL 0.1% formic acid in water and subjected to LC-MS/MS analysis.

LC-MS/MS analysis. An UltiMate 3000 RSLCnano system (Thermo Fisher Scientific) and Orbitrap Fusion Lumos (Thermo Fisher Scientific) were utilized for LC-MS/MS analysis. The analysis employed a nano-HPLC capillary column (ODS, 75 µm i.d. × 120 mm, particle size: 3.0 µm, Nikkyo Technos Co Ltd, Tokyo, Japan). A linear gradient of 2-35% mobile phase B (0.1% formic acid in acetonitrile) over 120 min was utilized for peptide separation, with mobile phase A consisting of 0.1% formic acid in water. Following peptide elution, the gradient was ramped to 95% mobile phase B over 2 min and held for 23 min to wash the column. Subsequently, the gradient was ramped to 5% mobile phase A over 0.1 min and held for 10 min to re-equilibrate the column. Data acquisition was performed using an Orbitrap Fusion Lumos mass

Cellular Physiology and Biochemistry

Cell Physiol Biochem 2024;58:292-310

DOI: 10.33594/000000713
Published online: 8 July 2024

© 2024 The Author(s). Published by
Cell Physiol Biochem Press GmbH&Co. KG

297

Suttinont et al.: Neurotrophic Release Control by Piezo2

spectrometer. Separated peptides were electrosprayed with a potential of 1.8 kV applied at the Nanospray Flex NG source while the ion transfer tube was maintained at 275°C. The ion funnel RF level was 30, the MS1 Orbitrap resolution was set at 60, 000 (at m/z 200) with a 380-1500 m/z range, and the MS1 AGC target and the maximum injection time were set at 4×10^5 and 50 ms. A data-dependent acquisition mode was employed to trigger precursor isolation and sequencing. Precursor ions with charges ranging from +2 to +7 were isolated for MS2 sequencing. ITMS2 spectra were collected with a rapid scan rate over a maximum injection time of 35 ms. The MS2 isolation window was 1.6 Da, the AGC target was 1×10^4, and the dynamic exclusion time was 60 s. For the Orbitrap Fusion Lumos MS, precursors were fragmented by higher energy collision-induced dissociation with a normalized collision energy of 30%. Mass calibration was automatically performed with a lock mass system using the peaks of m/z = 391.2843 and 445.12 for every injection.

MS data analysis and statistical analysis. All raw LC-MS/MS analysis used Proteome Discoverer (version 2.5) for feature detection, database searching, and protein/peptide quantification. Sequest and Amanda databases were utilized for the search, with MS/MS spectra searched against the Swiss-Prot and TrEMBL human databases. Dynamic modifications such as N-terminal protein acetylation and methionine oxidation were considered, while carbamidomethylation of cysteine residues was treated as a static modification. Precursor and fragment mass tolerances were set at 10 ppm and 0.02 Da, respectively. Peptides with a minimum length of seven amino acids and a maximum peptide mass of 5000 Da were considered, with up to two missed cleavages allowed per peptide. The second peptide search was activated to identify co-eluting and co-fragmented peptides from a single MS/MS spectrum. Peptide identification was validated using the Fixed Value PSM Validator Maximum (Delta Cn 0.05), and peptides and proteins were filtered with a maximum false discovery rate (FDR) of 0.01. Label-free quantitation (LFQ) calculations were performed separately for each parameter group containing similar cell loadings, utilizing unique and razor peptides for protein quantification. Other parameters were set to the default setting in Proteome Discoverer. Additionally, statistical analyses were conducted within Proteome Discoverer, with missing values imputed by random numbers drawn from a normal distribution (width, 0.3; downshift, 2.8). GO terms were annotated to the identified proteins using Perseus software (version 2.0.3.1).

ELISA

Supernatants from differentiated HSCs cultured in 24-well plates were replaced with hypotonic (Hypo) or isotonic (Iso) solutions and incubated at 37°C for 10 min. The concentration of secreted brain-derived neurotrophic factor (BDNF) was assessed using a Human BDNF SimpleStep ELISA (Enzyme-Linked Immuno Sorbent Assay) kit (ab212166, Abcam), which was performed according to the manufacturer's instructions. In brief, 50 µl of the medium obtained after osmotic induction was used as a sample. Subsequently, 50 µl of the antibody cocktail provided in the kit was added to the sample, and the resulting mixture was dispensed into 96-well plates pre-coated with the corresponding antibodies. Optical density (OD) measurements were recorded at a light intensity of 450 nm. The concentration of the samples was determined by constructing a standard curve.

Statistics

All data are expressed as means ± SEM measured from at least three independent experiments for each condition. Statistical significance was evaluated using Student's t-test to compare two mean values, with a significance threshold set at $*p < 0.05$, $**p < 0.01$. For Figs. 2c, 4f, 5c and 7, statistical differences in the data were evaluated with one-way analysis of variance followed by Tukey's test for multiple comparisons and was considered significant at $*p < 0.05$. For the analysis of cellular responses in Ca^{2+} imaging experiments, a chi-square test was conducted to evaluate the association between two categorical variables, with a value of $*p < 0.05$ considered significant. ns not significant.

Cellular Physiology and Biochemistry

Cell Physiol Biochem 2024;58:292-310

DOI: 10.33594/000000713
Published online: 8 July 2024

© 2024 The Author(s). Published by
Cell Physiol Biochem Press GmbH&Co. KG

298

Suttinont et al.: Neurotrophic Release Control by Piezo2

Results

Expression of Mechanosensitive Channels in Undifferentiated and Differentiated IFRS1 SCs

Recent investigations have highlighted the functions of SCs in response to mechanical stress, including their role in maintaining peripheral nerve axons, facilitating mechanical nociception and tactile sensation [4, 19]. In light of those findings, our study aimed to identify the expression of mechanosensitive channels in undifferentiated and in differentiated IFRS1 SCs and to explore their functional significance in this context.

When IFRS1 SCs were cultured in differentiation medium instead of undifferentiated medium, significant differences in their gene expression patterns emerged. Specifically, the expression levels of Krox20 and Myelin Basic Protein (Mbp) were significantly upregulated in differentiated IFRS1 SCs but there was no significant difference in the expression levels of p75Ntr between those two conditions (Fig. 1a). These findings are consistent with previous reports [15, 20] and suggest that the choice of culture medium results in distinct subtypes of SCs, namely non-myelinating and myelinating SCs.

Furthermore, our investigation assessed candidate mechanosensitive channels, as reported in previous studies, which included Piezo1/ Piezo2 [5], Trpv4 [6], Trpm7 [7, 8], and Trpa1 [9, 10]. Our results revealed the presence of Piezo1, Piezo2, and Trpm7 channels in differentiated IFRS1 SCs, while Trpv4 and Trpa1 channels were conspicuously absent in those cells (Fig. 1b). Importantly, differentiated IFRS1 SCs exhibited a significantly higher rate of increase in Piezo2 and Trpm7 channel expression compared to undifferentiated SCs (Fig. 1c). This pivotal observation underscores the central role of mechanosensitive channels within differentiated SCs.

Fig. 1. qPCR analysis of SC-related markers and mechanosensitive channels in undifferentiated and in differentiated IFRS1 SCs. (a) Expression changes of differentiation markers in undifferentiated (UnDiff.) and in differentiated (Diff.) IFRS1 SCs. Expression levels of p75Ntr and Krox20 are markers associated with Schwann cell precursor and pre-myelinated states, respectively, while Mbp indicates differentiated SCs. (b) Piezo1, Piezo2, Trpm7, Trpv4 and Trpa1 channels in differentiated IFRS1 SCs were examined using qRT-PCR. Data represent relative mRNA quantity compared to the control gene (β-actin). Data are expressed as means ± SE. (c) Expression levels of mechanosensitive channels (TRP and Piezo channels) in undifferentiated and in differentiated IFRS1 SCs. Data were normalized to the control gene (β-actin) and are presented as fold differences relative to UnDiff. IFRS1 SCs (n = 6). Error bars indicate SE.
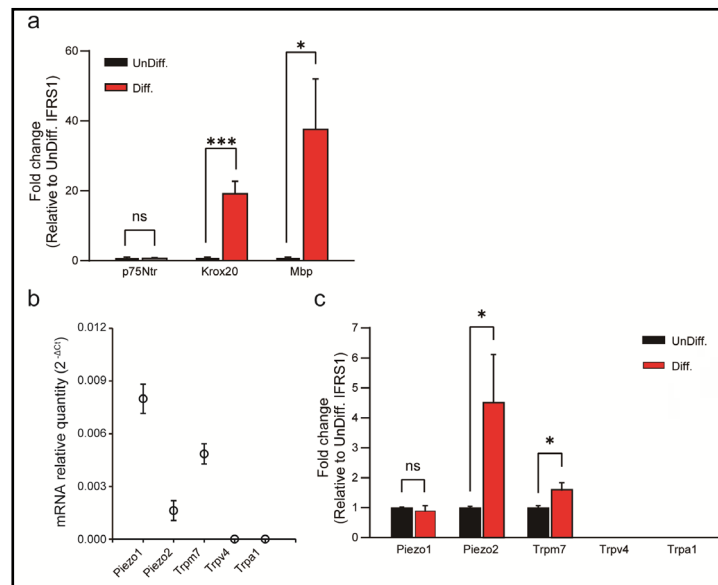
Hypotonicity Induces Ca^{2+} Transients in IFRS1 SCs through Mechanosensitive Channels
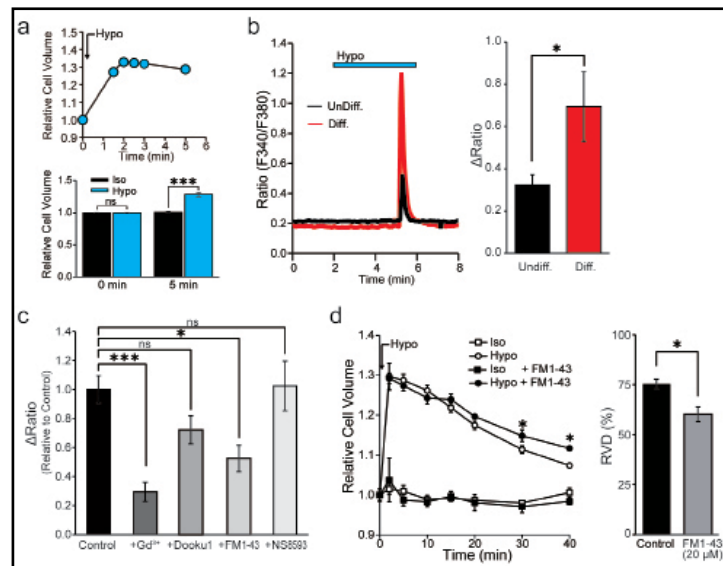
Recent reports have substantiated the presence of physiological responses in mechanosensitive cells, exemplified by Merkel cells [21] and dorsal root ganglion (DRG) neurons [22], when subjected to mechanical stimulation. Specifically, when exposed to mechanical forces, such as those resulting from cell swelling induced by hypotonic conditions, these cells activate mechanosensitive ion channels, most notably Piezo2 and Trpm7 channels. This activation is closely linked to alterations in membrane tension [23-25]. Furthermore, these mechanical stimuli trigger Ca^{2+}-permeable mechanosensitive ion channels, leading to a consequential increase in intracellular calcium concentration ($[Ca^{2+}]_i$).

In our study, we sought to characterize the mechanisms governing the regulation of Ca^{2+} concentration. To achieve that, we measured $[Ca^{2+}]_i$ in response to hypotonic stimulation in IFRS1 SCs. We initially verified the induction of cell swelling in IFRS1 SCs that results from exposure to a hypotonic solution. This validation was achieved by monitoring changes in cell volume following the initiation of hypotonicity-induced cell swelling. Notably, the hypotonic solution caused an expansion in cell volume, consistent with the Boyle-Vant Hoff law [26]. The average cell volume exhibited an initial regulatory volume decrease (RVD) but cell swelling remained at 5 min ($\sim$128.7 ± 3.3%) (Fig. 2a). Therefore, in this study, we adopted hypotonic stimulation conditions within 5 min, in which mechanical stimulation could be expected due to cell swelling, and then proceeded with the experiment.

Fig. 2b demonstrates the impact of hypotonicity-induced cell swelling for 4 min, revealing an increase in $[Ca^{2+}]_i$, expressed as the ΔRatio, both in undifferentiated and in differentiated IFRS1 SCs. Remarkably, the elevated ΔRatio value is notably more pronounced in differentiated IFRS1 SCs. Additionally, the cellular response to hypotonic stimulation was increased by 150.8%* (n = 328-413) compared to undifferentiated IFRS1 SCs.

Expanding upon our prior investigations into mechanosensitive ion channel expression in differentiated IFRS1 SCs, as shown in Fig. 1, we assessed the effects of established mechanosensitive channel inhibitors. The inhibitors used were: Gd^{3+}, a conventional mechanosensitive channel inhibitor [21]; Dooku1, a Piezo1 channel-specific inhibitor [27]; FM1-43, a potential inhibitor of Piezo2 channels [28], and NS8593, a selective inhibitor of Trpm7 channels [29]. Fig. 2c and Table 1 demonstrate that the hypotonicity-induced increase in the ΔRatio and the cellular response in differentiated IFRS1 SCs was significantly mitigated

Fig. 2. Cell volume and intracellular Ca^{2+} changes in differentiated IFRS1 SCs after hypotonic stimulation. (a) (upper) Representative example of continuous measurement of cell volume changes induced by hypotonic solution (Hypo). (bottom) Relative cell volume indicates the cell volume after exposure to isotonic (Iso) or hypotonic (Hypo) solutions at 5 min (n = 8). (b) Representative profile of intracellular Ca^{2+} indicated by the F340/F380 ratio in undifferentiated (UnDiff.) and in differentiated (Diff.) IFRS1 SCs. The blue bar at the top indicates exposure to hypotonic solution (n = 11). (c) Effects of channel blockers, Gd^{3+} (30 μM), Dooku1 (20 μM), FM1-43 (20 μM) and NS8593 (30 μM) on the fold change in the ΔRatio normalized to the value of hypotonicity-induced Ca^{2+} elevation in the absence of the respective reagent in Diff. IFRS1 SCs (n = 9-357). (d) Left, time course of the relative cell volume change of Diff. IFRS1 SCs in isotonic and in hypotonic solutions with or without FM1-43 (20 μM). Right, summary data showing RVD 40 min after application of hypotonic solution (n = 6-20). Error bars indicate SE.

Cellular Physiology and Biochemistry

Cell Physiol Biochem 2024;58:292-310

DOI: 10.33594/000000713
Published online: 8 July 2024

© 2024 The Author(s). Published by
Cell Physiol Biochem Press GmbH&Co. KG

300

Suttinont et al.: Neurotrophic Release Control by Piezo2

by Gd^{3+} and FM1-43. In contrast, no significant difference of the ΔRatio was observed when Dooku1 or NS8593 were used. These findings support the inference that the response of differentiated IFRS1 SCs to hypotonic solutions is predominantly mediated through Piezo2 channels.

Moreover, to elucidate the physiological role of Piezo2 in the mechanism of cell volume regulation, we quantified changes in cell volume following isotonic and hypotonic stimulation. The relative cell volume increased immediately after exposure of SCs to the hypotonic solution, reaching maximum swelling within 1 min. Following that initial peak, the relative cell volume decreased around 75% in the next 40 min by RVD (Fig. 2d). Treatment with FM1-43 impeded the cell volume recovery by around 20% during continuous exposure to hypotonic stimulation in IFRS1 SCs (Fig. 2d). These results suggest that Piezo2 mediates Ca^{2+} transients and is implicated in cell volume regulation in IFRS1 SCs.

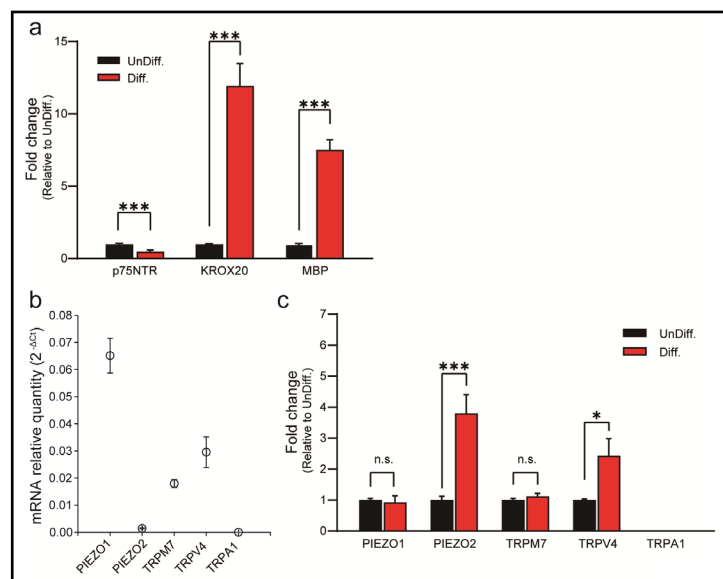### Expression of Mechanosensitive Channels in Primary HSCs

Next, we conducted quantitative polymerase chain reaction (qPCR) analysis to investigate the expression of PIEZO2 in HSCs. We induced HSC differentiation and assessed the expression of well-established SC differentiation markers, specifically p75NTR, KROX20 and MBP, using qPCR. The expression of those markers provided compelling evidence of successful differentiation of SCs (Fig. 3a)[15].
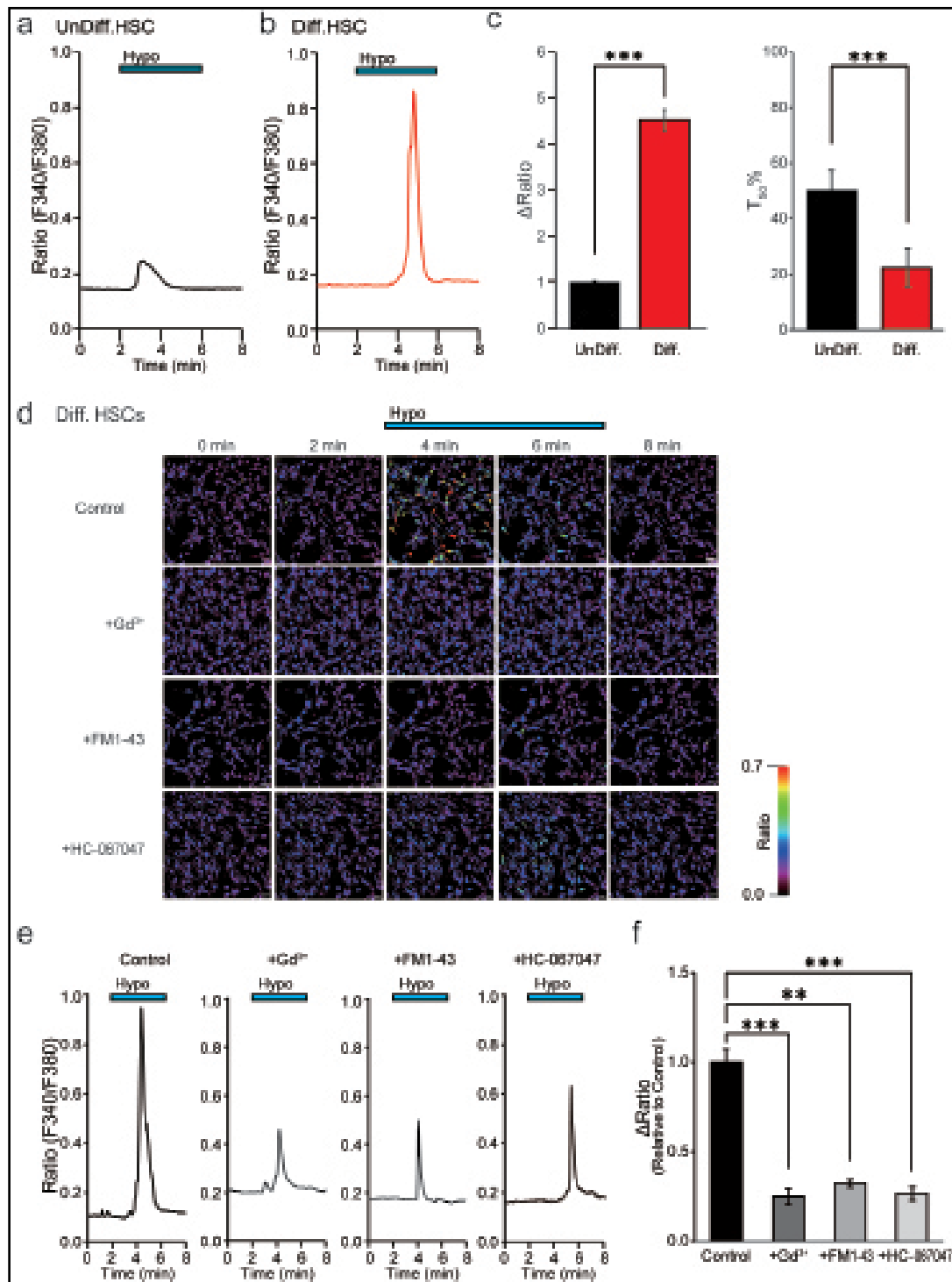
Subsequently, we examined the expression of mechanosensitive ion channels, mirroring the approach employed in our previous experiments conducted with IFRS1 SCs. Fig. 3b shows that PIEZO1, PIEZO2, TRPM7 and TRPV4 were expressed in differentiated HSCs. Interestingly, we observed a significant elevated expression of PIEZO2 and TRPV4 in differentiated HSCs compared to undifferentiated HSCs, while the elevated expression levels of PIEZO1, TRPM7 and TRPA1 remained comparatively low (Fig. 3c). The expression of TRPV4 was consistent with prior research studies (Fig. 3b) [6].

Table 1. The ΔRatio and cellular response rate of mechanosensitive ion channels in SCs. The effect of inhibitors of mechanosensitive ion channels on the ΔRatio and cellular response rate on hypotonicity-induced Ca^{2+} responses in IFRS1 SCs. The ΔRatio and cellular response rate for SCs treated with each inhibitor (Gd^{3+}, Dooku1, FM1-43, and NS8593) represents the normalized value compared to the control (n = 9-357)

Inhibitors	ΔRatio	Cellular response rate
Control	100.0 %	100.0 %
Gd^{3+}	29.3 %***	12.7 %***
Dooku1	72.2 %	87.7 %
FM1-43	52.7 %*	73.3 %*
NS8593	102.4 %	44.4 %*

Fig. 3. qPCR analysis of SC-related markers and mechanosensitive channels in undifferentiated and in differentiated HSCs. (a) Expression changes of differentiation markers in UnDiff. and in Diff. HSCs. Expression levels of p75NTR and KROX20 are markers associated with SC precursors and pre-myelinated states, respectively, while MBP indicates differentiated SCs. (b) PIEZO1, PIEZO2, TRPM7, TRPV4, and TRPA1 channels in differentiated HSCs were measured using RTq-PCR. Data represent relative mRNA quantity compared to the control gene (GAPDH). Data are expressed as means ± SE. (c) Expression levels

of mechanosensitive channels (TRP and PIEZO channels) in UnDiff. and in Diff. HSCs. Data were normalized to the control gene GAPDH and are presented as fold differences relative to UnDiff. HSCs (n = 5). Error bars indicate SE.

Cellular Physiology and Biochemistry

Cell Physiol Biochem 2024;58:292-310

DOI: 10.33594/000000713
Published online: 8 July 2024

© 2024 The Author(s). Published by
Cell Physiol Biochem Press GmbH&Co. KG

301

Suttinont et al.: Neurotrophic Release Control by Piezo2

Fig. 4. Effect of mechanosensitive ion channel inhibitors on hypotonicity-induced Ca^{2+} responses in HSCs by Ca^{2+} imaging. (a,b) Representative profile of intracellular Ca^{2+} indicated by the F340/F380 ratio in UnDiff. (a) and in Diff. (b) HSCs. The blue bar at the top indicates hypotonic stimulation (Hypo). (c) Bar graph showing the average value of the ΔRatio value and the half value of the decay time (T_{50}) of the data obtained in the experiments shown in a and b. (d) Effects of mechanosensitive ion channel inhibitors, Gd^{3+} (30 µM), FM1-43 (20 µM) and HC-067047 (1 µM). Representative intracellular Ca^{2+} imaging signals at 0, 2, 4, 6 and 8 min in Diff. HSCs induced by hypotonic solution. Scale bar = 50 µm. (e) Average signal obtained from analysis of the signals in d is shown. The blue bars at the top indicate exposure to hypotonic solutions. (f) Bar graph showing the average ΔRatio value of the data obtained from d and e. Effects of Gd^{3+}, FM1-43, and HC-067047 on hypotonicity-induced Ca^{2+} transients. Data are expressed as ΔRatios normalized to differentiated HSCs (Diff) as control (n = 17-543). Error bars indicate SE.

Ca^{2+} Dynamics in response to hypotonic stimulation in differentiated HSCs

To investigate the functional expression of PIEZO2 in undifferentiated and in differentiated HSCs, Ca^{2+} imaging was employed. Fig. 4a shows that the hypotonicity-induced cell swelling of undifferentiated HSCs substantially increased the $[Ca^{2+}]_i$ due to the characteristic transient Ca^{2+} influx, revealing a peak within 5 min. Specifically, a more pronounced effect was observed in differentiated HSCs, and the inactivation time from the peak of $[Ca^{2+}]_i$ elevation to a 50% decrease was 50.0 ± 7.5 s for undifferentiated HSCs and 22.4 ± 6.9 s for differentiated HSCs (Fig. 4a,b,c). Fig. 4c demonstrates a substantial increase in the ΔRatio of differentiated HSCs compared to undifferentiated HSCs. Additionally, the cellular response rate to hypotonic solution increased by 178.6%* compared with undifferentiated cell controls (n = 972-1800). The $[Ca^{2+}]_i$ profile in differentiated SCs mirrors that of Piezo1/2 in chondrocytes [30], which is distinct from the brief activation time observed for Trpv4 in undifferentiated mouse SCs [6].

To characterize the involvement of specific mechanosensitive channels, Gd^{3+}, FM1-43 and HC-067047 were administered before the hypotonic stimulation, considering the upregulation of PIEZO2 and TRPV4 in differentiated HSCs compared to undifferentiated HSCs (see Fig. 3b). The effects of those inhibitors did not affect the basal ΔRatio value under isotonic solution conditions for 10 min (n = 152). As shown in Figs. 4d, e and f, Gd^{3+}, FM1-43, and HC-067047 significantly attenuated the ΔRatio compared to the control. Conversely, the cellular response rate to hypotonic solution was inhibited by Gd^{3+} and FM1-43 but not by HC-067047 compared to the control (Table 2).

Furthermore, the role of PIEZO2 was elucidated by confirmation of knockdown effects using siRNAs targeting PIEZO2 and TRPV4 in differentiated HSCs (Fig. 5). Compared to mock-treated cells, siRNA-treated cells targeting PIEZO2 or TRPV4 exhibited a significant suppression of the ΔRatio (Fig. 5c). In contrast, cellular responses were not suppressed in TRPV4 siRNA-treated cells, whereas suppression was observed in PIEZO2 siRNA-treated cells compared to the control (Table 2). These findings are consistent with the results of drug inhibition using HC-067047 performed in previous experiments (Figs. 4d, e, f). Taken together, the results demonstrate that PIEZO2 plays a more significant role than TRPV4 in responding to hypotonic solutions.

Considering these observations, it is reasonable to hypothesize that part of the steep $[Ca^{2+}]_i$ rise in the response of differentiated HSCs to hypotonic solution relies on the mediation of PIEZO2 channels.
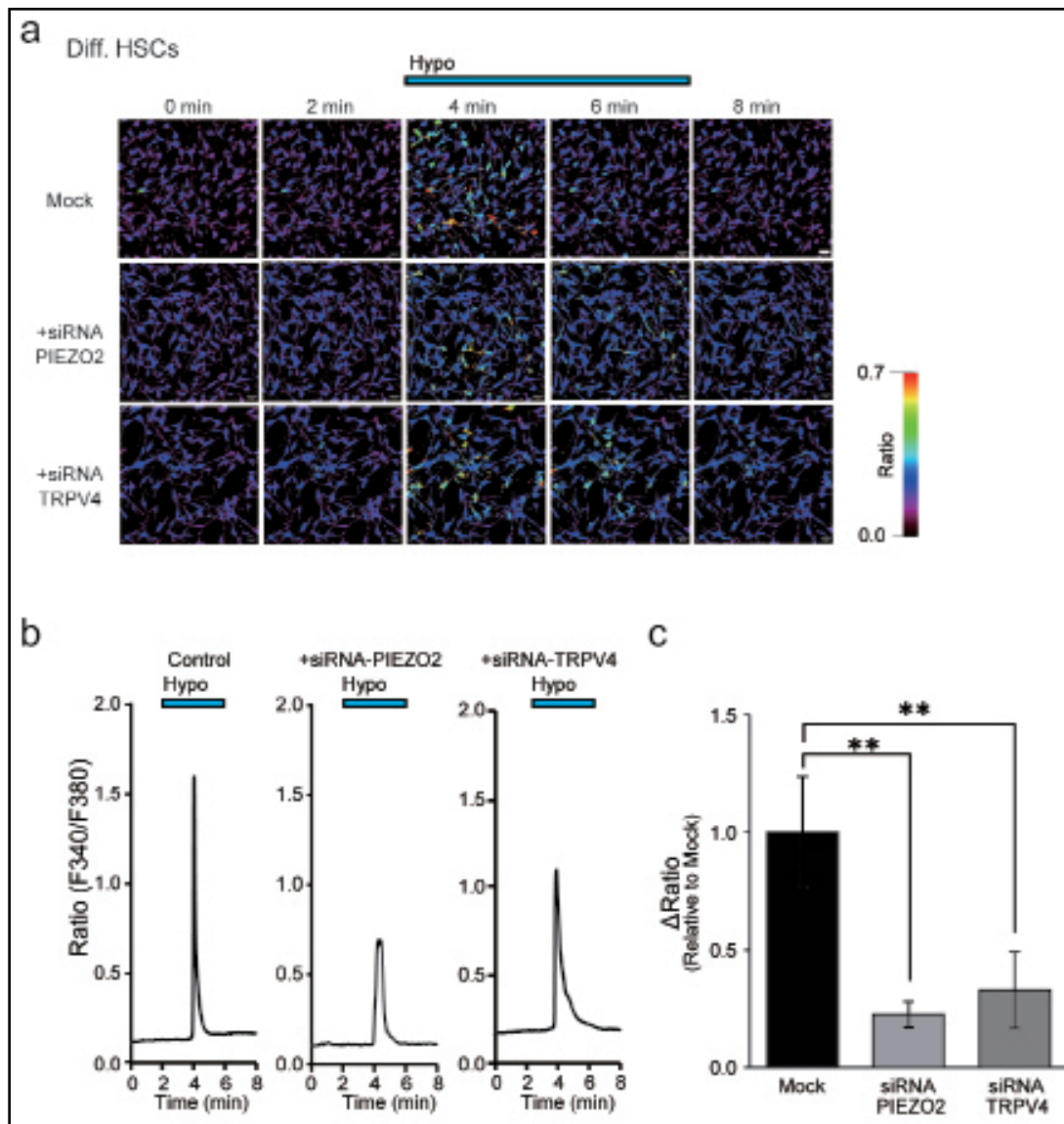
Immunohistochemical Confirmation of PIEZO2 Expression in HSCs

Figs. 4 and 5 show that our functional assessment results unequivocally establish PIEZO2 expression in differentiated HSCs. An immunostaining experiment (Fig. 6a) demonstrates that 75.0% of MBP-positive SCs after the induction of differentiation co-express PIEZO2, contrasting markedly with the 0.7% co-expression of PIEZO2 in MBP-negative cells. Furthermore, Western blotting data in (Fig. 6b, left) reveal a significant increase in PIEZO2 expression in differentiated HSCs, showing an increase of $288 \pm 94.1\%$ compared to undifferentiated HSCs. As a positive control, an immunoreactive band with a molecular weight of approximately 250 kDa was detected in PIEZO2-overexpressing cells (Fig. 6b, right). This finding is consistent with a previous report [31].

In summary, these findings collectively underscore the high expression of functional PIEZO2 in differentiated HSCs and highlight its potential importance in this cellular context.

Augmented Secretion of BDNF Following Mechanical Stimulation

We subsequently explored the impact of mechanical stimulation on the secretome of HSCs by discovering proteomic analysis using LC-MS/MS. Analysis targeting nerve/axonal growth factors identified 89 candidate secretion-related proteins that were upregulated 20% or more after 10 min of hypotonic stimulation compared to an isotonic solution

Cellular Physiology and Biochemistry

Cell Physiol Biochem 2024;58:292-310

DOI: 10.33594/000000713
Published online: 8 July 2024

© 2024 The Author(s). Published by
Cell Physiol Biochem Press GmbH&Co. KG

303

Suttinont et al.: Neurotrophic Release Control by Piezo2

Fig. 5. Effect of Piezo2 siRNA on hypotonicity-induced Ca^{2+} responses in differentiated HSCs by Ca^{2+} imaging. (a) Effects of siRNAs for PIEZO2 or TRPV4 on Diff. HSCs. Representative intracellular Ca^{2+} imaging signals induced by hypotonic solution (Hypo) at 0, 2, 4, 6, and 8 min. (b) Averaged signals obtained from the analyses of a are shown. The blue bar at the top indicates exposure to hypotonic stimulation. Scale bar = 50 μm. (c) Bar graph showing the average ΔRatio value of the data obtained in images shown in a and b. Data are expressed as ΔRatios normalized to Mock as a control (n = 101-197). Error bars indicate SE.

(Supplementary Table 1). Among those proteins, we focused on BDNF, given its crucial role in promoting nerve growth and regeneration in response to mechanical stimulation of SCs and its quantifiability via ELISA.

There was an increase in BDNF levels from 10.6 to 14.1 pg/ml* (n = 39-40) after 10 min of exposure of SCs maintained under isotonic solution conditions to hypotonic conditions. The relative BDNF secretion significantly increased compared to standardize data collected across multiple sets.

To investigate further whether PIEZO2 mediates the secretion of these factors, we excluded Gd^{3+} and FM1-43, which were used in previous experiments, due to potential measurement uncertainty for secretion stimuli. Namely, the potential secretory effects induced by long-term administration of Gd^{3+} [32] and the pigmentary properties of FM1-

Cellular Physiology and Biochemistry

Cell Physiol Biochem 2024;58:292-310

DOI: 10.33594/000000713
Published online: 8 July 2024

© 2024 The Author(s). Published by
Cell Physiol Biochem Press GmbH&Co. KG

304

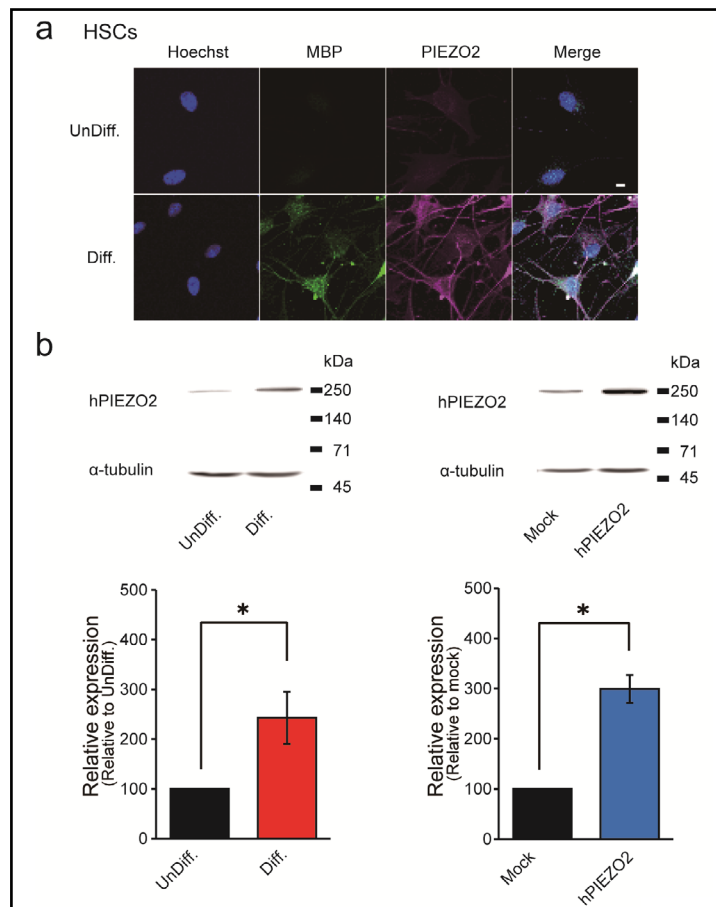Suttinont et al.: Neurotrophic Release Control by Piezo2

43 [33] have been reported. Instead, we employed siRNA-mediated knockdown in this experiment.

Firstly, Mock siRNA-treated HSCs showed increased BDNF secretion upon hypotonic stimulation (Fig. 7, gray bars), which agreed with the 10-min exposure to hypotonic conditions in the control experiment. Next, in an inhibition experiment using PIEZO2 siRNA treatment, BDNF secretion from PIEZO2 siRNA-treated HSCs was significantly increased compared to the control (Fig. 7, pink bars). Notably, BDNF secretion after hypotonic stimulation increased even more with PIEZO2 siRNA than with mock siRNA. However, this secretory-promoting effect of PIEZO2 siRNA was not observed in comparison with Mock siRNA in an isotonic solution.

Table 2. The ΔRatio and cellular response rate of mechanosensitive ion channels in HSCs. The effect of inhibitors or siRNAs of mechanosensitive ion channels on the ΔRatio and cellular response rate on hypotonicity-induced Ca^{2+} responses in HSCs. The ΔRatio and cellular response rate for HSCs treated with each inhibitor (Gd^{3+}, FM1-43, and HC-067047) or siRNAs (targeting PIEZO2 and TRPV4) represents the normalized value compared to control or siRNA mock, respectively (n = 641-1800)

Inhibitors / siRNA	ΔRatio	Cellular response rate
Control	100.0 %	100.0 %
Gd^{3+}	25.1 %*	21.7 %*
FM1-43	32.4 %**	30.0 %*
HC-067047	26.7 %***	96.4 %
Mock	100 %	100 %
siPIEZO2	20.0 %**	65.4 %*
siTRPV4	30.0 %**	95.5 %

Fig. 6. Immunohistochemical analysis of PIEZO2 expression in HSCs (a) Representative confocal laser fluorescence microscopy images in HSCs co-stained with Hoechst (blue), MBP (green) and PIEZO2 (magenta). Scale bar = 50 μm. (b) Western blot analysis of α-tubulin and PIEZO from UnDiff. and from Diff. HSCs (left) and HSCs transfected with hPIEZO2 (hPIEZO2) or vector (Mock) (right). Data are representative results. Bar graph showing the relative value of PIEZO2 protein expression in Diff. HSCs or PIEZO2 overexpression (n = 4), with UnDiff. HSCs or Mock as 100%. Error bars indicate SE.

Cellular Physiology and Biochemistry

Cell Physiol Biochem 2024;58:292-310

DOI: 10.33594/000000713
Published online: 8 July 2024

© 2024 The Author(s). Published by
Cell Physiol Biochem Press GmbH&Co. KG

305

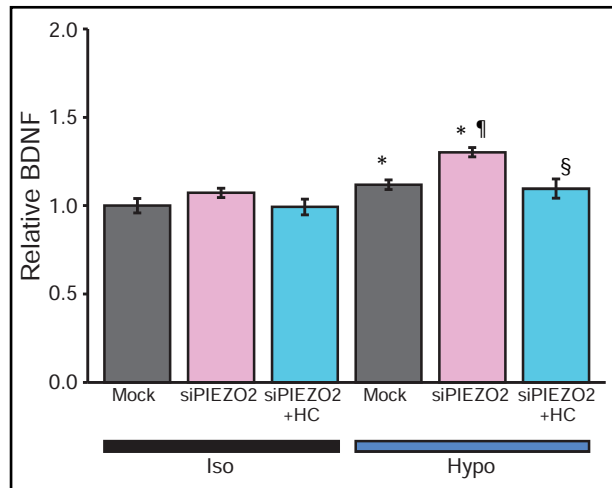Suttinont et al.: Neurotrophic Release Control by Piezo2

To explore the secretion-promoting effect of PIEZO2 siRNA following hypotonic stimulation of HSCs, we investigated the involvement of TRPV4, which was previously investigated in SCs [6]. The inhibition of TRPV4 using HC-067047 suppressed the hypotonicity-induced secretion of BDNF to the same level as isotonic condition (Fig. 7, blue bars). These findings suggest a role for PIEZO2 as a negative regulator of TRPV4 in hypoosmotic HSC secretion.

In summary, the upregulation of BDNF secretion after hypotonic stimulation slows cell swelling time, as observed in the Piezo2 deficiency in SCs (Fig. 2). This implies that Ca^{2+} influx through TRPV4 increases, leading to the enhanced secretion of BDNF. These findings highlight the potential role of PIEZO2 as a finely tuned regulator of neurotrophic factor secretion by HSCs in response to mechanical stimulation, which is essential for neural function and regenerative processes.

Fig. 7. BDNF secretion from differentiated HSCs in hypotonic solution using ELISA. Effects of siRNA negative control treated cells (Mock), siRNA PIEZO2 (siPIEZO2) treated cells, and the presence of HC-067047 (HC). Mean relative values of isotonic (Iso) or hypotonic (Hypo) solution-induced secretion of BDNF (n = 39-40). Error bars indicate SE. *p<0.05, **p<0.01 vs Iso or Mock-Iso, ¶p<0.05 vs Mock-Hypo, §p<0.05 vs siPIEZO2-Hypo.

Discussion

This study has made significant findings regarding the functional expression and amplified physiological responses of PIEZO2 following the induction of differentiation in HSCs and in IFRS1 SCs. Our results underscore the involvement of PIEZO2, at least in part, in the RVD response to hypotonic stimuli, and suggest an indirect influence on the amount of BDNF released by regulating the cell swelling duration.

The expression analysis of Ca^{2+}-permeable mechanosensitive channels in undifferentiated and in differentiated IFRS1 SCs revealed the expression of Piezo1, Piezo2 and TRPM7 (Fig. 1), which is consistent with prior reports [5, 7, 8]. Intriguingly, TRPV4 and TRPA1 expression was not previously reported [6, 9, 10]. Subsequently, our investigation was extended to HSCs, utilizing highly purified cells provided by Dr. Monje [15, 16]. The mechanosensitive channel expression analysis in undifferentiated and in differentiated HSCs yielded results in line with previous reports, confirming the presence of Piezo1, Piezo2 [5], TRPM7 [7, 8], and TRPV4 [6] (see Fig. 3a). Notably, while previous studies have reported the presence of TRPA1 both in rat SCs and in HSCs [9, 10], our analysis did not detect TRPA1 expression (Figs. 1b and 3b). This discrepancy may be due to variations in the sources of HSCs, as commercially available HSCs are often contaminated with fibroblasts and have distinct properties compared to highly purified HSCs [34]. Additionally, the observed differences in TRPV4 expression in mice [6] and TRPA1 expression in HSCs [10] and rats [9] suggest that variations in species, SC immortalization and differences in differentiation stages might contribute to this inconsistency. The expression of TRPM7 was observed to increase with differentiation in rat IFRS1 SCs (Fig. 1b). This suggests a heightened demand for elevated levels of TRPM7 expression during the cell differentiation process into more specialized cell types and their subsequent functions post-differentiation. Indeed, the significance of TRPM7 during and post-differentiation processes has been noted in various

tissues, such as bone [35], where its function contributes to mechanosensation alongside its RVD capability [24]. Recently, the involvement of Piezo2 in itching was shown in mice, yet no evidence indicates that a PIEZO2 deficiency affects itch sensitivity in humans [36, 37]. Indeed, recognizing the species differences between rats and humans suggests that further investigations are essential before extrapolating concepts from animal models to humans [15, 34]. Future studies are warranted to comprehensively elucidate the underlying reasons for these distinct expression patterns.

Our results indicate that PIEZO2 and TRPV4 mediate the ΔRatio and cellular responses to hypotonic solutions of HSCs. This conclusion is supported by the inhibitory effects of Gd^{3+}, FM1-43 and siRNA-PIEZO2, as well as HC-067047 and siRNA-TRPV4 on TRPV4 (Figs. 4d-f, 5, and Table 2). Interestingly, while the inhibition of Piezo2 and TRPV4 caused a marked decrease in the ΔRatio, inhibition of TRPV4 did not result in a statistically significant decrease in cells responding to hypotonicity (Table 2). These findings suggest that PIEZO2 is involved in the transient Ca^{2+} rise in response to membrane stretching during hypotonicity-induced cell swelling, whereas TRPV4 is responsible for the sustained intracellular Ca^{2+} rise when swelling is prolonged. This is consistent with previous reports on the nature of ion channel activity [38, 39]. Furthermore, our results demonstrated that a physiological role for sustained Ca^{2+} influx through TRPV4 is suitable for a regulator of secretion such as BDNF (Fig. 7b).

Interestingly, a delayed response characteristic of Ca^{2+} transient behavior was observed in IFRS1 SCs and HSCs, as depicted in Figs. 2b and 4a, b, e. As demonstrated in Fig. 2a, when the cell volume increased by approximately 30% due to hypoosmotic cell swelling for about 2 min, the membrane stretching might have surpassed the pressure threshold for Piezo2 to respond to mechanical stimulation. This nuanced response underscores the necessity for a comprehensive understanding of the precise mechanisms governing Ca^{2+} signaling in HSCs, particularly concerning the potential interaction of Piezo2 channels with other modulators.

During development and maturity, SCs in peripheral nerves are subject to various mechanical stresses such as tension, compression and shear strain. Accumulating evidence supports the claim that substances secreted by SCs contribute significantly to the growth, maintenance, and regeneration of peripheral nerves [40, 41].

Utilizing secretome analysis through LC-MS/MS, our study unveiled dynamic changes in the levels of more than 80 factors following a 10 min exposure to hypotonic stimulation, as detailed in Supplementary Table 1. Those results include factors that have been reported as crucial for SC proliferation and myelination, e.g., Ski oncogene [42], glypican [43], Wnt5 [44] and related to neural regeneration; e.g., Neuropilin2 [45] and vascular endothelial growth factor A [46].

Among the factors implicated in biological processes, BDNF is a typical neurotrophin known to promote various neural responses through specific cell surface receptor binding [47, 48]. Our ELISA measurements corroborated these findings, indicating an increased secretion of BDNF upon mechanical stimulation (Fig. 7).

On the other hand, attention should be paid to the novel factors associated with tumor or neurodegenerative disease progression that are secreted together with growth-related factors following exposure to hypotonic solution (Supplementary Table 1): Tumor necrosis factor receptor superfamily member 12A [49], and neurologically related diseases are in that list, along with Proto-oncogene tyrosine-protein kinase Src, which is involved in neuropathic pain [50], Presenilin-1, which has been verified as a causative factor for early onset Alzheimer's disease [51], and Huntingtin-associated protein 1, Huntingtin interacting protein [52].

Our results suggest that the hypotonic solution-induced secretion levels in HSCs may have a negative correlation with Piezo2 and tumor progression, as well as the secretion of neural-related factors. These findings prompt further investigation into the potential implications of hypotonic solution-induced secretion levels in HSCs in the development and progression of tumors and neurodegenerative diseases.

Cellular Physiology and Biochemistry

Cell Physiol Biochem 2024;58:292-310

DOI: 10.33594/000000713
Published online: 8 July 2024

© 2024 The Author(s). Published by
Cell Physiol Biochem Press GmbH&Co. KG

307

Suttinont et al.: Neurotrophic Release Control by Piezo2

Upon inhibition of Piezo2, the RVD mechanism is hindered, leading to cell volume swelling. This can be understood by recognizing the extension of the loading time of mechanical stimulation (Fig. 2d). The prolonged loading time can cause excessive secretion by HSCs, due to sustained TRPV4-mediated $[Ca^{2+}]_i$ elevation, as shown in Fig. 7.

It is worth noting that while TRPV4 is expressed in HSCs (Fig. 1b), it is not detected in IFRS1 SCs (Fig. 3b). This difference may be explained by the fact that other Ca^{2+}-permeable mechanosensors, such as TRPM7 [24, 53], TRPC1 [54], Piezo1 [55] and TMEM63B [56], have been previously identified as contributing to the regulation of RVD. Therefore, it is possible that these alternative mechanisms, depending on the animal species and the stage of differentiation, may work cooperatively with Piezo2 to regulate RVD in a complementary manner. While our study advances understanding of the mechanosensors involved in RVD, ongoing research remains essential to comprehensively unravel the intricate regulatory mechanisms governing cell volume dynamics in HSCs.

Conclusion

In conclusion, our study revealed the expression and mechanosensitive function of Piezo2 in human primary SCs, especially in differentiated SCs that respond to hypotonic stimuli by releasing neurotrophic factors. These findings provide new insights into the mechanotransduction processes governing SC behavior and their potential role in neural regeneration and maintenance. Further studies are required to elucidate the precise mechanisms and signaling pathways underlying these observations and to harness SC mechanotransduction for therapeutic intervention in neurologically related diseases.

Acknowledgements

Statement of Ethics
Primary HSC cultures were obtained from postmortem human peripheral nerves made available as deidentified (coded) biospecimens by the National Disease Research Interchange (NDRI) and the Life Alliance Organ Recovery Agency (LAORA) of the University of Miami Miller School of Medicine to the laboratories of Paula Monje and Patrick Wood at The Miami Project to Cure Paralysis, respectively. NDRI and LAORA strictly adhere to government regulations and guidelines regarding donor authorization and confidentiality and ensure that informed consent is obtained from the donors (or the next-of-kin thereof) for research use. *In vitro* experimentation in this project was approved and deemed to constitute non-human subjects research by the Human Subjects Research Offices of the University of Miami and Indiana University. The study protocol has been further reviewed and approved by the

Ethics Committee of Shiseido MIRAI Institute in accordance with the National Institutes of Health Guidelines and the Declaration of Helsinki Principles (C10424).

Disclosure Statement

CS, MY, KM and MT are employees of Shiseido Co., Ltd., Japan.

References

1   Salzer JL: Switching myelination on and off. The Journal of cell biology 2008;181:575-577.
2   Sango K: Novel neuron-Schwann cell co-culture models to study peripheral nerve degeneration and regeneration. Neural regeneration research 2023;18:1732-1733.
3   Abdo H, Calvo-Enrique L, Lopez JM, Song J, Zhang MD, Usoskin D, El Manira A, Adameyko I, Hjerling-Leffler J, Ernfors P: Specialized cutaneous Schwann cells initiate pain sensation. Science (New York, NY) 2019;365:695-699.
4   Ojeda-Alonso J, Calvo-Enrique L, Paricio-Montesinos R, Kumar R, Zhang MD, Poulet JFA, Ernfors P, Lewin GR: Sensory Schwann cells set perceptual thresholds for touch and selectively regulate mechanical nociception. Nature communications 2024;15:898.
5   Acheta J, Bhatia U, Haley J, Hong J, Rich K, Close R, Bechler ME, Belin S, Poitelon Y: Piezo channels contribute to the regulation of myelination in Schwann cells. Glia 2022;70:2276-2289.
6   Feng X, Takayama Y, Ohno N, Kanda H, Dai Y, Sokabe T, Tominaga M: Increased TRPV4 expression in non-myelinating Schwann cells is associated with demyelination after sciatic nerve injury. Communications biology 2020;3:716.
7   Chun YL, Kim M, Kim YH, Kim N, Yang H, Park C, Huh Y, Jung J: Carvacrol effectively protects demyelination by suppressing transient receptor potential melastatin 7 (TRPM7) in Schwann cells. Anatomical science international 2020;95:230-239.
8   Kim YH, Lee S, Yang H, Chun YL, Kim D, Yeo SG, Park C, Jung J, Huh Y: Inhibition of transient receptor potential melastatin 7 (TRPM7) protects against Schwann cell trans-dedifferentiation and proliferation during Wallerian degeneration. Animal cells and systems 2020;24:189-196.
9   De Logu F, De Siena G, Landini L, Marini M, Souza Monteiro de Araujo D, Albanese V, Preti D, Romitelli A, Chieca M, Titiz M, Iannone LF, Geppetti P, Nassini R: Non-neuronal TRPA1 encodes mechanical allodynia associated with neurogenic inflammation and partial nerve injury in rats. British journal of pharmacology 2023;180:1232-1246.
10   De Logu F, Li Puma S, Landini L, Portelli F, Innocenti A, de Araujo DSM, Janal MN, Patacchini R, Bunnett NW, Geppetti P, Nassini R: Schwann cells expressing nociceptive channel TRPA1 orchestrate ethanol-evoked neuropathic pain in mice. The Journal of clinical investigation 2019;129:5424-5441.
11   Andersen ND, Monje PV: Isolation, Culture, and Cryopreservation of Adult Rodent Schwann Cells Derived from Immediately Dissociated Teased Fibers. Methods in molecular biology (Clifton, NJ) 2018;1739:49-66.
12   Eldridge CF, Bunge MB, Bunge RP, Wood PM: Differentiation of axon-related Schwann cells *in vitro*. I. Ascorbic acid regulates basal lamina assembly and myelin formation. The Journal of cell biology 1987;105:1023-1034.
13   Sobue G, Pleasure D: Schwann cell galactocerebroside induced by derivatives of adenosine 3',5'-monophosphate. Science (New York, NY) 1984;224:72-74.
14   Jessen KR, Mirsky R, Morgan L: Role of cyclic AMP and proliferation controls in Schwann cell differentiation. Annals of the New York Academy of Sciences 1991;633:78-89.
15   Monje PV, Sant D, Wang G: Phenotypic and Functional Characteristics of Human Schwann Cells as Revealed by Cell-Based Assays and RNA-SEQ. Molecular neurobiology 2018;55:6637-6660.
16   Peng K, Sant D, Andersen N, Silvera R, Camarena V, Piñero G, Graham R, Khan A, Xu XM, Wang G, Monje PV: Magnetic separation of peripheral nerve-resident cells underscores key molecular features of human Schwann cells and fibroblasts: an immunochemical and transcriptomics approach. Scientific reports 2020;10:18433.
17   Schneider CA, Rasband WS, Eliceiri KW: NIH Image to ImageJ: 25 years of image analysis. Nature methods 2012;9:671-675.

Cellular Physiology and Biochemistry

Cell Physiol Biochem 2024;58:292-310

DOI: 10.33594/000000713
Published online: 8 July 2024

© 2024 The Author(s). Published by
Cell Physiol Biochem Press GmbH&Co. KG

309

Suttinont et al.: Neurotrophic Release Control by Piezo2

18 Ferdoushi A, Jamaluddin MFB, Li X, Pundavela J, Faulkner S, Hondermarck H: Secretome analysis of human schwann cells derived from malignant peripheral nerve sheath tumor. Proteomics 2022;22:e2100063.

19 Cobo R, García-Piqueras J, García-Mesa Y, Feito J, García-Suárez O, Vega JA: Peripheral Mechanobiology of Touch-Studies on Vertebrate Cutaneous Sensory Corpuscles. International journal of molecular sciences 2020;21

20 Bacallao K, Monje PV: Requirement of cAMP signaling for Schwann cell differentiation restricts the onset of myelination. PloS one 2015;10:e0116948.

21 Haeberle H, Bryan LA, Vadakkan TJ, Dickinson ME, Lumpkin EA: Swelling-activated Ca2+ channels trigger Ca2+ signals in Merkel cells. PloS one 2008;3:e1750.

22 Yamaguchi S, Otsuguro K: A mechanically activated ion channel is functionally expressed in the MrgprB4 positive sensory neurons, which detect stroking of hairy skin in mice. Neuroscience letters 2017;653:139-145.

23 Jia Z, Ikeda R, Ling J, Viatchenko-Karpinski V, Gu JG: Regulation of Piezo2 Mechanotransduction by Static Plasma Membrane Tension in Primary Afferent Neurons. The Journal of biological chemistry 2016;291:9087-9104.

24 Numata T, Shimizu T, Okada Y: TRPM7 is a stretch- and swelling-activated cation channel involved in volume regulation in human epithelial cells. American journal of physiology Cell physiology 2007;292:C460-467.

25 Numata T, Shimizu T, Okada Y: Direct mechano-stress sensitivity of TRPM7 channel. Cellular physiology and biochemistry : international journal of experimental cellular physiology, biochemistry, and pharmacology 2007;19:1-8.

26 Hoffmann EK, Lambert IH, Pedersen SF: Physiology of cell volume regulation in vertebrates. Physiological reviews 2009;89:193-277.

27 Evans EL, Cuthbertson K, Endesh N, Rode B, Blythe NM, Hyman AJ, Hall SJ, Gaunt HJ, Ludlow MJ, Foster R, Beech DJ: Yoda1 analogue (Dooku1) which antagonizes Yoda1-evoked activation of Piezo1 and aortic relaxation. British journal of pharmacology 2018;175:1744-1759.

28 Villarino NW, Hamed YMF, Ghosh B, Dubin AE, Lewis AH, Odem MA, Loud MC, Wang Y, Servin-Vences MR, Patapoutian A, Marshall KL: Labeling PIEZO2 activity in the peripheral nervous system. Neuron 2023;111:2488-2501.e2488.

29 Chubanov V, Mederos y Schnitzler M, Meißner M, Schäfer S, Abstiens K, Hofmann T, Gudermann T: Natural and synthetic modulators of SK (K(ca)2) potassium channels inhibit magnesium-dependent activity of the kinase-coupled cation channel TRPM7. British journal of pharmacology 2012;166:1357-1376.

30 Lee W, Leddy HA, Chen Y, Lee SH, Zelenski NA, McNulty AL, Wu J, Beicker KN, Coles J, Zauscher S, Grandl J, Sachs F, Guilak F, Liedtke WB: Synergy between Piezo1 and Piezo2 channels confers high-strain mechanosensitivity to articular cartilage. Proceedings of the National Academy of Sciences of the United States of America 2014;111:E5114-5122.

31 Romero LO, Caires R, Kaitlyn Victor A, Ramirez J, Sierra-Valdez FJ, Walsh P, Truong V, Lee J, Mayor U, Reiter LT, Vásquez V, Cordero-Morales JF: Linoleic acid improves PIEZO2 dysfunction in a mouse model of Angelman Syndrome. Nature communications 2023;14:1167.

32 Thinnes FP, Hellmann KP, Hellmann T, Merker R, Schwarzer C, Walter G, Götz H, Hilschmann N: Studies on human porin XXI: gadolinium opens Up cell membrane standing porin channels making way for the osmolytes chloride or taurine-A putative approach to activate the alternate chloride channel in cystic fibrosis. Molecular genetics and metabolism 2000;69:240-251.

33 Betz WJ, Mao F, Bewick GS: Activity-dependent fluorescent staining and destaining of living vertebrate motor nerve terminals. The Journal of neuroscience : the official journal of the Society for Neuroscience 1992;12:363-375.

34 Monje PV: The properties of human Schwann cells: Lessons from *in vitro* culture and transplantation studies. Glia 2020;68:797-810.

35 Shin M, Mori S, Mizoguchi T, Arai A, Kajiya H, Okamoto F, Bartlett JD, Matsushita M, Udagawa N, Okabe K: Mesenchymal cell TRPM7 expression is required for bone formation via the regulation of chondrogenesis. Bone 2023;166:116579.

36 Feng J, Duan B: Understanding neural mechanisms of mechanical itch. The Journal of allergy and clinical immunology 2023;152:32-35.

310

37   Szczot M, Nickolls AR, Lam RM, Chesler AT: The Form and Function of PIEZO2. Annual review of biochemistry 2021;90:507-534.

38   Soattin L, Fiore M, Gavazzo P, Viti F, Facci P, Raiteri R, Difato F, Pusch M, Vassalli M: The biophysics of piezo1 and piezo2 mechanosensitive channels. Biophys Chem 2016;208:26-33.

39   Vriens J, Watanabe H, Janssens A, Droogmans G, Voets T, Nilius B: Cell swelling, heat, and chemical agonists use distinct pathways for the activation of the cation channel TRPV4. Proceedings of the National Academy of Sciences of the United States of America 2004;101:396-401.

40   Belin S, Zuloaga KL, Poitelon Y: Influence of Mechanical Stimuli on Schwann Cell Biology. Frontiers in cellular neuroscience 2017;11:347.

41   Jeanette H, Marziali LN, Bhatia U, Hellman A, Herron J, Kopec AM, Feltri ML, Poitelon Y, Belin S: YAP and TAZ regulate Schwann cell proliferation and differentiation during peripheral nerve regeneration. Glia 2021;69:1061-1074.

42   Atanasoski S, Notterpek L, Lee HY, Castagner F, Young P, Ehrengruber MU, Meijer D, Sommer L, Stavnezer E, Colmenares C, Suter U: The protooncogene Ski controls Schwann cell proliferation and myelination. Neuron 2004;43:499-511.

43   Chernousov MA, Rothblum K, Stahl RC, Evans A, Prentiss L, Carey DJ: Glypican-1 and alpha4(V) collagen are required for Schwann cell myelination. The Journal of neuroscience : the official journal of the Society for Neuroscience 2006;26:508-517.

44   Yu F, Weng J, Yuan YS, Kou YH, Han N, Jiang BG, Zhang PX: Wnt5a Affects Schwann Cell Proliferation and Regeneration via Wnt/c-Jun and PTEN Signaling Pathway. Chinese medical journal 2018;131:2623-2625.

45   Ara J, Bannerman P, Shaheen F, Pleasure DE: Schwann cell-autonomous role of neuropilin-2. Journal of neuroscience research 2005;79:468-475.

46   Cattin AL, Burden JJ, Van Emmenis L, Mackenzie FE, Hoving JJ, Garcia Calavia N, Guo Y, McLaughlin M, Rosenberg LH, Quereda V, Jamecna D, Napoli I, Parrinello S, Enver T, Ruhrberg C, Lloyd AC: Macrophage-Induced Blood Vessels Guide Schwann Cell-Mediated Regeneration of Peripheral Nerves. Cell 2015;162:1127-1139.

47   Zhang JY, Luo XG, Xian CJ, Liu ZH, Zhou XF: Endogenous BDNF is required for myelination and regeneration of injured sciatic nerve in rodents. The European journal of neuroscience 2000;12:4171-4180.

48   Boyd JG, Gordon T: Neurotrophic factors and their receptors in axonal regeneration and functional recovery after peripheral nerve injury. Molecular neurobiology 2003;27:277-324.

49   Liao M, Liao J, Qu J, Shi P, Cheng Y, Pan Q, Zhao N, Zhang X, Zhang L, Tan Y, Li Q, Zhu JF, Li J, Zhang C, Cai SY, Chai J: Hepatic TNFRSF12A promotes bile acid-induced hepatocyte pyroptosis through NFκB/Caspase-1/GSDMD signaling in cholestasis. Cell death discovery 2023;9:26.

50   Cai Y, Xu J, Cheng Q: Proto-oncogene tyrosine-protein kinase SRC (Src) inhibition in microglia relieves neuroinflammation in neuropathic pain mouse models. Bioengineered 2021;12:11390-11398.

51   Do HN, Devkota S, Bhattarai A, Wolfe MS, Miao Y: Effects of presenilin-1 familial Alzheimer's disease mutations on γ-secretase activation for cleavage of amyloid precursor protein. Communications biology 2023;6:174.

52   Wu LL, Zhou XF: Huntingtin associated protein 1 and its functions. Cell adhesion & migration 2009;3:71-76.

53   Numata T, Sato-Numata K, Hermosura MC, Mori Y, Okada Y: TRPM7 is an essential regulator for volume-sensitive outwardly rectifying anion channel. Communications biology 2021;4:599.

54   Madsen CP, Klausen TK, Fabian A, Hansen BJ, Pedersen SF, Hoffmann EK: On the role of TRPC1 in control of Ca2+ influx, cell volume, and cell cycle. American journal of physiology Cell physiology 2012;303:C625-634.

55   Sforna L, Michelucci A, Morena F, Argentati C, Franciolini F, Vassalli M, Martino S, Catacuzzeno L: Piezo1 controls cell volume and migration by modulating swelling-activated chloride current through Ca(2+) influx. Journal of cellular physiology 2022;237:1857-1870.

56   Du H, Ye C, Wu D, Zang YY, Zhang L, Chen C, He XY, Yang JJ, Hu P, Xu Z, Wan G, Shi YS: The Cation Channel TMEM63B Is an Osmosensor Required for Hearing. Cell reports 2020;31:107596.